EDGE ARTICLE

Photoswitchable dynasore analogs to control endocytosis with light†

Núria Camarero, [ID] ‡[a] Ana Trapero,‡[ab] Ariadna Pérez-Jiménez,[a] Eric Macia,[c] Alexandre Gomila-Juaneda,[a] Andrés Martín-Quirós,[a] Laura Nevola,§[d] Artur Llobet,[e] Amadeu Llebaria,[b] Jordi Hernando, [ID] [f] Ernest Giralt [ID] [dg] and Pau Gorostiza [ID] *[ahi]

The spatiotemporal control of cellular dynamic processes has great fundamental interest but lacks versatile molecular tools. Dynamin is a key protein in endocytosis and an appealing target to manipulate cell trafficking using patterns of light. We have developed the first photoswitchable small-molecule inhibitors of endocytosis (dynazos), by a stepwise design of the photochromic and pharmacological properties of dynasore, a dynamin inhibitor. We have characterized their photochromism with UV-visible and transient absorption spectroscopy and their biological activity using fluorescence microscopies and flow cytometry. Dynazos are water-soluble, cell permeable, and photostable, and enable fast, single-wavelength photoswitchable inhibition of clathrin-mediated endocytosis at micromolar concentration.

Introduction

Most of the proteins in the cell require the interaction with other molecules or proteins to play their biological function. These interactions are crucial for the proper control of a wide variety of cellular processes, such as cell division, membrane trafficking, signaling, *etc.* A way to understand how these cellular processes work is by perturbing the activity of one key component in the system and observing how the process is affected by this perturbation. Small molecules can be used to interfere with the biological function of a protein, by inhibiting or activating their function. These compounds are a powerful tool to probe the molecular mechanisms involved in the transduction of specific biological signals and lead to the development of novel therapeutic strategies.[1] Potency and selectivity to a target protein subtype are desirable qualities to avoid off-target effects, since the stronger the binding and its

consequences, the longer they last and the more difficult they are to revert. Compared to genetic approaches to interfere with the action of a protein, such as RNAi or the overexpression of dominant negative proteins, the use of small molecules offers several advantages in terms of controlling the dynamics and reversibility of the response. The effects of overexpressing a protein can take hours or days to appear and could be irreversible, whereas small molecules are often fast acting and can be readily removed. Acute stimulation with these compounds can also prevent the development of homeostatic or compensatory mechanisms by the cell, which plague the outcomes and interpretation of genetic manipulations.[2]

Local administration of compounds can further improve their efficacy and the reversibility of the elicited responses, *e.g.* when studying the pharmacological profile of an ion channel with electrophysiological recordings and fast perfusion of selective inhibitors.[3] However, the use of diffusible molecules poses limitations on the temporal and spatial precision that can be achieved. Once the molecule is administered, it can be diluted or distributed in tissue, and the control on spatial location and precise timing of its activity is lost.

This is important when investigating transient or irreversible events (*e.g.* the cellular processes involved in membrane trafficking) or when disturbing the activity of proteins essential for cell survival (whose consequences could be extended to other cells or tissues).[4,5] These limitations can also affect the efficacy and specificity of drugs used in pharmacotherapy. As an example, the cytotoxic anti-neoplastic agents used in cancer treatment result in severe side effects due to the lack of specificity towards healthy tissue.[6]

These problems can be addressed with compounds whose biological activity can be turned on and off remotely and

[a]*Institute for Bioengineering of Catalonia (IBEC), The Barcelona Institute of Science and Technology (BIST), Spain. E-mail: pau@icrea.cat*

[b]*Institute for Advanced Chemistry of Catalonia (IQAC-CSIC), Spain*

[c]*Institut de Pharmacologie Moléculaire et Cellulaire (IPMC), Université Nice Sophia Antipolis, France*

[d]*Institute for Research in Biomedicine (IRB Barcelona), Spain*

[e]*Bellvitge Biomedical Research Institute (IDIBELL), Spain*

[f]*Departament de Química, Universitat Autònoma de Barcelona (UAB), Spain*

[g]*Universitat de Barcelona (UB), Spain*

[h]*CIBER-BBN, Spain*

[i]*ICREA, Spain*

† Electronic supplementary information (ESI) available. See DOI: 10.1039/d0sc03820b

‡ NC and AT contributed equally.

§ Present address: IDP Discovery Pharma, Parc Científic de Barcelona (PCB), Spain.

reversibly, like light-regulated drugs used in photo-pharmacology. These molecules can be obtained by the introduction of a light-sensitive group (photoswitch) in the structure of a biologically active ligand.[5,7] Careful molecular design and extensive testing allow in some cases to use light as the external trigger to control the drug's pharmacologic activity with high spatiotemporal resolution.[8] The azobenzene is one of the best-studied photoswitchable groups for this purpose and has been extensively used in photopharmacology to regulate the activity of ion channels,[3,9–11] G protein-coupled receptors,[12,13] and enzymes.[14,15] It undergoes a *trans/cis* isomerization process upon irradiation with ultraviolet (UV) light, which can be reverted by illumination with visible light or by thermal relaxation of the less stable *cis* isomer.[16] This results in light-induced changes of the molecular length, geometry and dipolar moment, which can be exploited to alter the pharmacological properties of an appended bioactive moiety.

Among all fundamental biological processes, endocytosis greatly exemplifies both the interest and challenges to manipulate the cellular spatiotemporal dynamics. It is used by all eukaryotic cells to internalize extracellular material along with portions of the plasma membrane through the formation of vesicles. It regulates many physiological processes, including the uptake of nutrients, growth factors and transmembrane receptors and it also constitutes the entry pathway of a variety of pathogens.[17] There are many different routes of endocytosis operating at the same time at the cell surface,[18] which are critical in controlling the membrane turnover and plasticity in essential cellular functions such as mitosis, cell differentiation, adhesion, migration, and transmembrane receptor signaling. Endocytic processes involve the concerted action of many proteins, complexes, cell membranes and compartments, and constitute potential targets to prevent infections and to kill cells.

Although the main molecular players of endocytosis are well characterized, and several experimental methods have been developed to observe their dynamics, the molecular mechanisms are far from being understood due in part to the lack of acute manipulation tools.[19,20] One of the key molecular players involved in most endocytic pathways is dynamin, a GTPase required for membrane scission during the endocytic vesicle formation.[21,22]

Dynamin is essential not only for clathrin-mediated endocytosis (CME), one of the best-characterized endocytic pathways which is dependent on the recruitment of clathrin cages to the membrane, but also for other clathrin-independent routes for cellular endocytosis.[23,24] The GTPase activity of dynamin represents a highly efficacious target to control endocytosis and a growing number of small molecules that specifically inhibit dynamin activity have been described.[25–29] Nowadays these inhibitors constitute not only useful research tools for the study of endocytosis, but also a promising strategy for the treatment of viral and bacterial infections. Thus, dynamin is an appealing target to manipulate endocytosis in spatiotemporally designated patterns with light.

To photocontrol dynamin activity, we combined the pharmacological properties of the dynamin inhibitor dynasore[28]

(Fig. 1a) and the photochromic properties of an azobenzene group, to yield a series of photoswitchable analogues of dynamin inhibitors that we called dynazos (compounds dynazo-**2**, dynazo-**3** and dynazo-**4** in Fig. 1a). Here we present their design strategy, synthesis, and their photochromic and biological characterization.

Results and discussion

We decided to partially integrate azobenzene into the structure of dynasore as a constitutive part of the inhibitor pharmacophore (shaded in light blue in Fig. 1a). We expected that this might allow preservation of the inhibitory activity to an extent that was sensitive to the photoisomer configuration, thereby enabling control of inhibition with light. The number and the relative position of the hydroxyl groups in the catechol moiety of dynasore are important for its biological activity,[25,30] and for this reason the azobenzene unit was introduced at the position of the naphthyl fragment.

We had to take into account an additional constraint as an integral part of the design, namely that dynasore absorbs in the same spectral region as regular *trans*-azobenzenes[16] (~330 nm, Fig. 1b, black plot) and, as a result, it photodegrades upon continuous direct excitation with the UV light required for photoisomerization (*e.g.* 355 nm, ESI Fig. S1†). In order to decouple the absorption spectra of dynasore and the azobenzene moiety of the dyad, we selected azobenzene groups with red-shifted photoisomerization wavelengths, which have the additional advantages of deeper penetration than UV light and reduced cellular damage upon prolonged exposure.[31,32] It is reported that azobenzenes with strong electron-donating substituents at 2- or 4-position (*e.g.* –NH$_2$ or –OH) absorb at longer wavelengths and display fast thermal back isomerization to the *trans* configuration in the dark.[16,33]

We thus took advantage of the hydroxyl group present in the naphthyl moiety of the pharmacophore, which was preserved in the azobenzene core of the dynazo compounds designed in order to achieve the desired spectral red shift (Fig. 1a).

With these design principles in mind, we first synthesized dynazo-**2**, the simplest of the compounds prepared. Compared to dynasore, the UV-visible absorption spectrum of dynazo-**2** shows an additional absorption peak at 372 nm in phosphate buffer saline (PBS) that confirms successful red shift of the absorption spectrum of its azobenzene photochrome (violet solid plot in Fig. 1b). This bathochromic displacement is even more pronounced in DMSO, the lowest energy azobenzene absorption band appearing at 447 nm (dark blue solid plot in ESI Fig. S2†). Based on previous reports on 4-hydroxyazobenzenes, the larger spectral effect found in DMSO might be ascribed to intramolecular hydrogen bonding between the nearby hydroxyl and carbonyl substituents of the azo chromophore, which will not be favored in aqueous media.[34] Next, we tested if the biological activity of dynasore was retained in dynazo-**2**. A well-established method to study dynamin inhibitors on endocytosis is to measure receptor-mediated transferrin (Tf) uptake.[35] Fluorescently labeled Alexa 563-Tf was allowed to
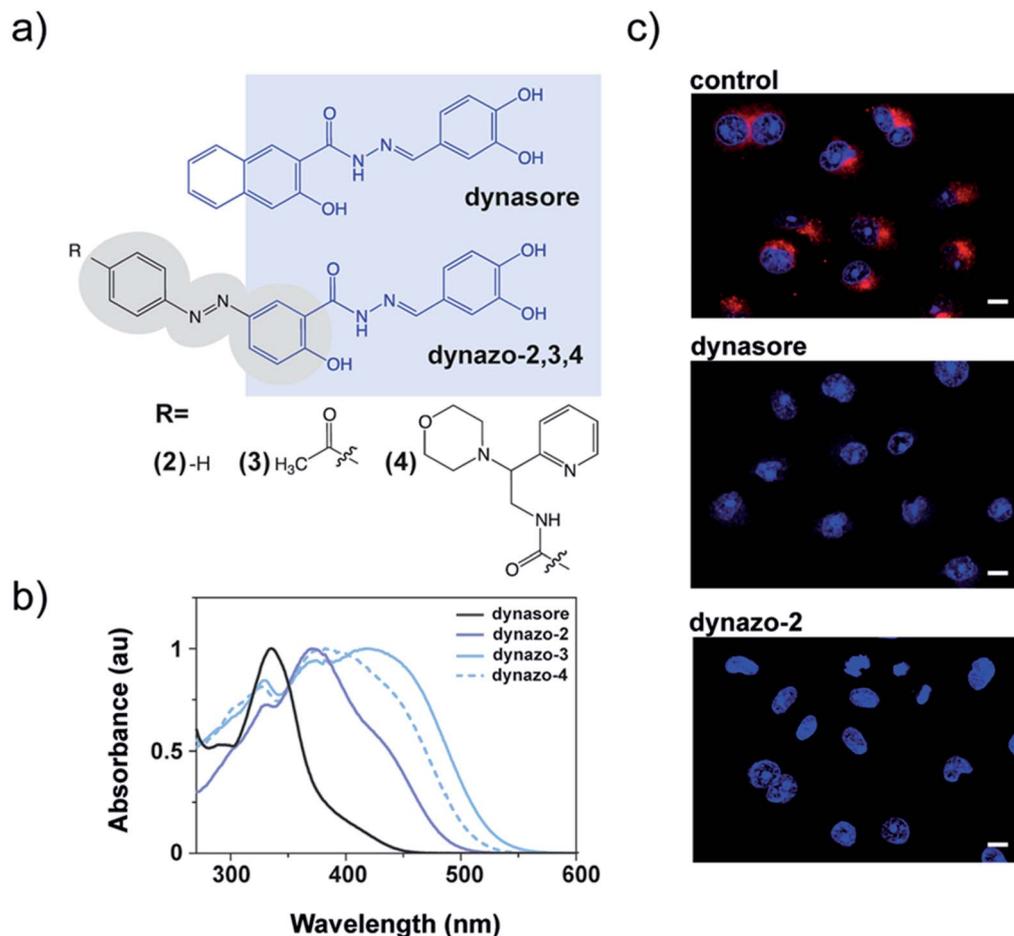
Fig. 1 Molecular design and biological activity of dynazos, photochromic dynasore analogs. (a) Chemical structures of dynasore, a well-known dynamin inhibitor,[28] and dynazos. Highlighted in blue, the structure of dynasore that has been conserved in the design of dynazos-2, 3 and 4. There are also shown the electron-withdrawing substituents introduced on the azobenzene core of dynazos-3 and 4 (gray ovals) to improve their photochromic and biological properties with respect to dynazo-2. (b) UV-visible absorption spectra in PBS with 1% DMSO showing the red-shifted azobenzene absorption of dynazos-2, 3 and 4 compared to dynasore upon incorporation of strong electron-donating and electron-withdrawing substituents. (c) Confocal microscopy images of transferrin (Tf) uptake assays in COS-7 cells. The uptake of Alexa-568-Tf (red) is inhibited in cells treated with dynazo-2 (100 μM) to a similar extent as in cells treated with dynasore (80 μM) compared to control vehicle-treated cells. DRAQ5 staining shows nuclei (blue) (scale bar: 10 μm).

bind to its endogenous receptor on the surface of COS-7 intact cells by incubation at low temperature to slow down endocytosis. After removal of the Tf excess, cells were transferred to 37 °C for 15 minutes to allow internalization of the Tf-receptor complex and cell surface-bound Tf was removed by an acidic wash. After nuclei staining and cell fixation, internalized Tf-receptor complexes accumulated at the perinuclear-recycling late endosomes and could be observed by fluorescence confocal microscopy (Fig. 1c). Incubation with dynazo-2 (100 μM) reduced Tf internalization to a similar extent than dynasore (80 μM) compared to control vehicle-treated cells (Fig. 1c). These results confirmed that our approach for the integration of the azobenzene moiety into the dynasore structure does not compromise its biological activity and prompted us to undertake further chemical modifications of the azobenzene core away from the pharmacophore to improve its photochromic response and activity modulation.

Two derivatives of dynazo-2 were thus designed and synthesized. Dynazo-3 has an acetyl group at the 4′-position of the azobenzene core (Fig. 1a). We introduced this electron-withdrawing group to generate a push–pull azobenzene derivative with an even larger absorption bathochromic shift with respect to dynazo-2. In addition, the incorporation of this group was also intended to reduce the affinity of the cis form towards dynamin by increasing the steric hindrance around the biologically active fragment of the compound upon photoisomerization. This design concept was further exploited in dynazo-4, where a much bulkier electron-withdrawing amide group was introduced. To facilitate chemical access to a variety of potential candidates, the ketone group was replaced by an amide to which several commercially available N-substituents could be attached. Importantly, this should not detrimentally affect the optical properties of the resulting compound (i.e. absorption red-shift), as proven by our spectroscopic

measurements. The N-(2-morpholino-2-(pyridin-2-yl)ethyl) amide substituent chosen for this purpose trades off steric hindrance and aqueous solubility, compared to other options. For instance, for an N-(2-diphenylethyl)amide group, we observed a strong reduction in aqueous solubility that essentially prevented biological experiments (data not shown in the manuscript). The photophysical properties of the new dynazos were again analyzed by UV-visible spectroscopy (Fig. 1b). Compared to parent compound dynazo-**2**, the substituents introduced in dynazo-**3** and dynazo-**4** caused an additional red shift of the absorption spectra, especially for dynazo-**3** (∼45 nm and ∼40 nm in PBS and DMSO respectively, Fig. 1d and ESI Fig. S2†).

The synthesis of dynazo-**4** was achieved as shown in Scheme 1. Diazotization of 4-aminobenzoic acid and coupling of the resulting diazonium salt with methyl 2-hydroxybenzoate yielded azobenzene **5**. The reaction of the obtained intermediated **5** with hydrazine hydrate led to the formation of acid hydrazide **6**, which underwent condensation with 3,4-dihydroxybenzaldehye affording hydrazine **7**. Finally, amide coupling of acid **7** and 2-morpholino-2-(pyridin-2-yl)ethanamine afforded dynazo-**4**.

As reported for azobenzene derivatives with strong meso-meric electro-donating and/or electron-withdrawing groups[33] dynazo-**2**, **3**, **4** displayed very fast cis to trans thermal isomeri-zation rates, which prevented observation of the photo-conversion of these switches using steady state UV-visible absorption spectroscopy. Instead, time-resolved absorption spectroscopy allowed recording with nanosecond accuracy the time evolution of the cis states formed after pulsed irradiation of these compounds.

Fig. 2 shows the transient absorption spectra measured for dynazo-**2**, **3**, **4** in PBS right after photoexcitation (ΔAbs at $t = 0$), which display negative values in all cases that must be attrib-uted to the light-induced conversion of their initial trans isomers into less absorbing species. This, together with the fast time decay of the negative ΔAbs signal to recover the initial situation, prove reversible trans/cis azobenzene

photoisomerization in dynazo-**2**, **3**, **4** and allow estimating the most efficient wavelengths to induce this process:[36] ca. 390 nm (dynazo-**2**) and 405 nm (dynazo-**3**, **4**) in PBS, which are in good agreement with the red-shifted absorption bands shown by these compounds with respect to dynasore in Fig. 1b. As such, photoexcitation of the azobenzene and dynasore units in dynazo-**2**, **3**, **4** could be decoupled, which should enable trans/cis photoisomerization without degrading their pharmaco-phore. This was demonstrated by illumination with violet light at 405 nm, which should lead to efficient photoisomerization. Remarkably, no photodegradation of dynasore or of any of the dynazos was observed under these excitation conditions (ESI Fig. S3†), thus confirming the success of our design approach.

In agreement with the behavior expected owing to their azobenzene substitution pattern, fast thermal back isomeriza-tion of the cis isomers of dynazo-**2**, **3**, **4** was clearly observed by monitoring the time evolution of transient absorption and the corresponding cis state lifetimes (τ) were determined by fitting monoexponential functions to the recorded data. As it is shown in the insets of Fig. 2b–d, dynazos' relaxation times are between 0.6 and 0.7 ms, confirming that these compounds back isom-erize to their trans configuration as soon as illumination is turned off. Continuous irradiation is thus required to maintain a significant fraction of cis isomers, which is advantageous to spatiotemporally constrain dynamin photoresponses regardless of compound diffusion, in contrast to the behavior of slow-relaxing diffusible compounds. In addition, fast-relaxing compounds also allow single-wavelength operation to control the target protein activity, thus simplifying the experimental resources needed.

To study the effect of dynazos on CME, we quantified the uptake of Alexa 488-labeled Tf by large populations of cells using flow cytometry. We used the same protocol than in the experiments of Fig. 1c, with cell resuspension in complete medium after the acidic wash, and propidium iodide staining to exclude dead cells from the analysis. The fluorescence of cells incubated in increasing amounts of each compound (ranging
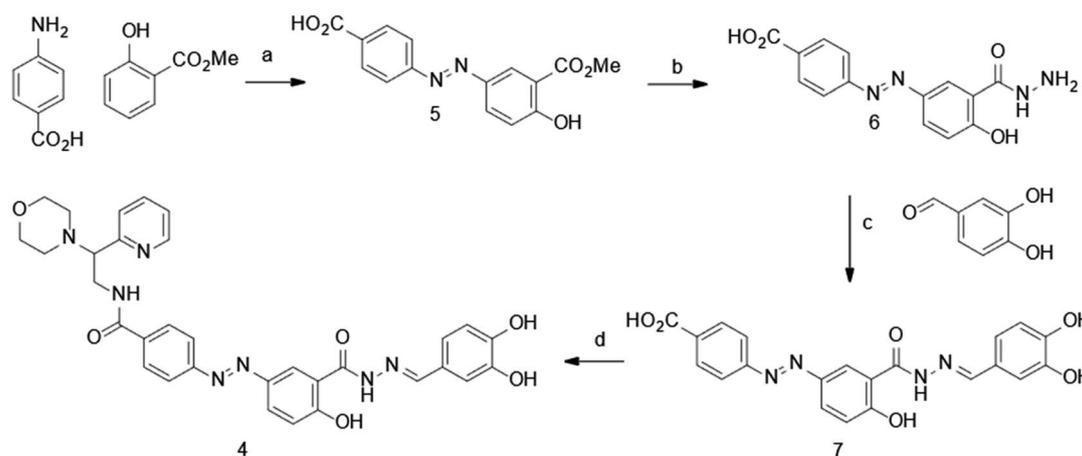
Scheme 1 Synthesis of dynazo-**4**. Reagents and conditions: (a) (i) NaNO$_2$ (1.1 eq.), HCl/H$_2$O (v/v = 8 : 92), −5 °C; (ii) NaOH (2 eq.), Na$_2$CO$_3$ (2 eq.), H$_2$O, −5 °C, 61% yield; (b) NH$_2$NH$_2$·H$_2$O (4 eq.), EtOH, reflux, 62% yield; (c) EtOH, reflux, 83% yield; (d) 2-morpholino-2-(pyridin-2-yl)ethanamine (1.2 eq.), EDC (1.5 eq.), HOBt (1.5 eq.), TEA (2.6 eq.), DMF, RT, 57% yield.
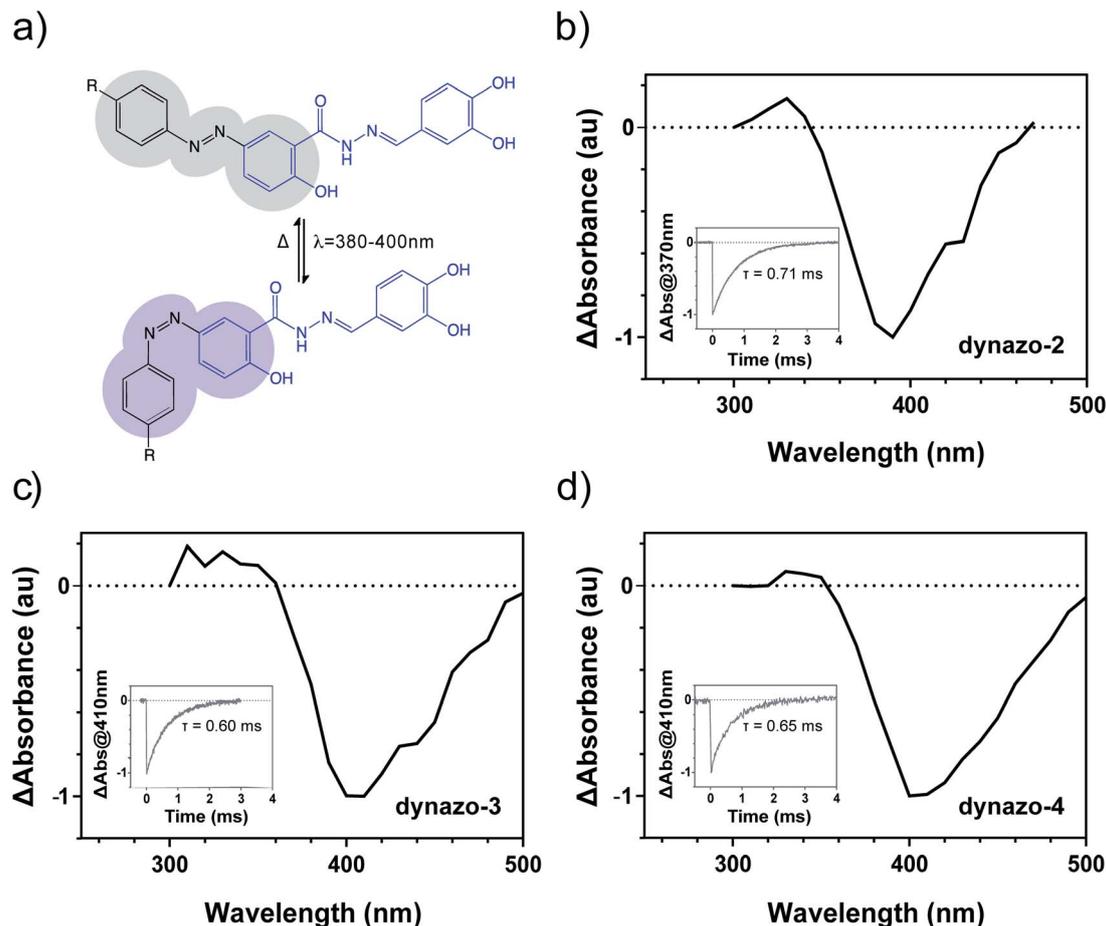
Fig. 2 Characterization of dynazos' photochromism. (a) Photoisomerization of dynazos occurs upon illumination of the thermally stable *trans* isomer (gray ovals) with a wavelength between *ca.* 350–450 nm. The *trans* isomer is recovered by thermal back isomerization of the *cis* isomer (violet ovals). Transient absorption spectra of (b) dynazo-**2**, (c) dynazo-**3** and (d) dynazo-**4** after nanosecond pulsed laser excitation ($\lambda = 355$ nm, $t = 0$) confirms efficient photoisomerization and bathochromic shift of the most efficient irradiation wavelength from 390 nm in dynazo-**2** to 405 nm in dynazo-**3**, **4**. The transient absorption decays and the thermal lifetimes of the *cis* isomers (τ) retrieved from monoexponential fits are shown in the insets of (b) dynazo-**2**, (c) dynazo-**3** and (d) dynazo-**4**. Measurements were conducted in PBS with 1% DMSO.

from 0.5 to 10 μM) was measured and plotted as a percentage of the mean fluorescence of vehicle-treated cells (Fig. 3a–c, black solid plots corresponding to dark conditions). These results confirm that photoisomerizable dynazos inhibit Tf uptake in a dose-dependent manner. To assess if the inhibitory activity of dynazos on CME could be remotely controlled with light, we repeated Tf uptake assays incubating dynazo-**2**, **3**, **4** in separate cell plates in the dark and under optimal illumination conditions in each case, *i.e.* 380 nm for dynazo-**2**, and 405 nm for dynazo-**3**, **4** (Fig. 3a–c). Control experiments showed no effect of light on Tf uptake assays performed in untreated cells (ESI Fig. S4 and Methods/ESI for further details†). A Tf uptake time-course in untreated cells is also shown in ESI Fig. S5† to show the progression of Tf internalization without addition of dynazos. The inhibitory activities of all dynazos displayed significant differences between dark and illuminated conditions, at concentrations of 1 μM for dynazo-**2** and between 0.5 μM and 5 μM for dynazo-**3** and dynazo-**4**. The greatest relative differences in the inhibitory activities between the two conditions are ~20% for 1 μM dynazo-**2**, **3** and ~35% for 1 μM dynazo-**4**. It

must be noted that flow cytometry measurements are performed in thousands of cells and that the significance of the observed differences is therefore very high (dynazo-**2**, $P < 0.005$, dynazo-**3**, $P < 0.0001$ and dynazo-**4**, $P < 0.0005$; 1 μM concentration, two-tailed *t*-test).

Having determined the useful operating conditions, we further characterized the effect of illumination in Tf uptake using confocal microscopy. We performed Alexa-563-Tf uptake assays as in Fig. 1c but separately incubating cells in the dark and under illumination (405 nm) in the presence of 1 μM dynazo-**4**. Representative confocal microscopy images of this experiment are shown in Fig. 3d. In Fig. 3e, the average fluorescence intensities of 112 to 153 cells for each condition are plotted relative to the control dark condition (100% internalization). Dynazo-**4** significantly reduced Tf uptake by 47% ($P < 0.0163$) in the dark compared to the 405 nm illumination conditions or to vehicle-incubated controls, in good agreement with the cytometry experiments of Fig. 3c. These results demonstrate that CME can be remotely controlled in intact, untransfected cells by means of small molecules (photochromic
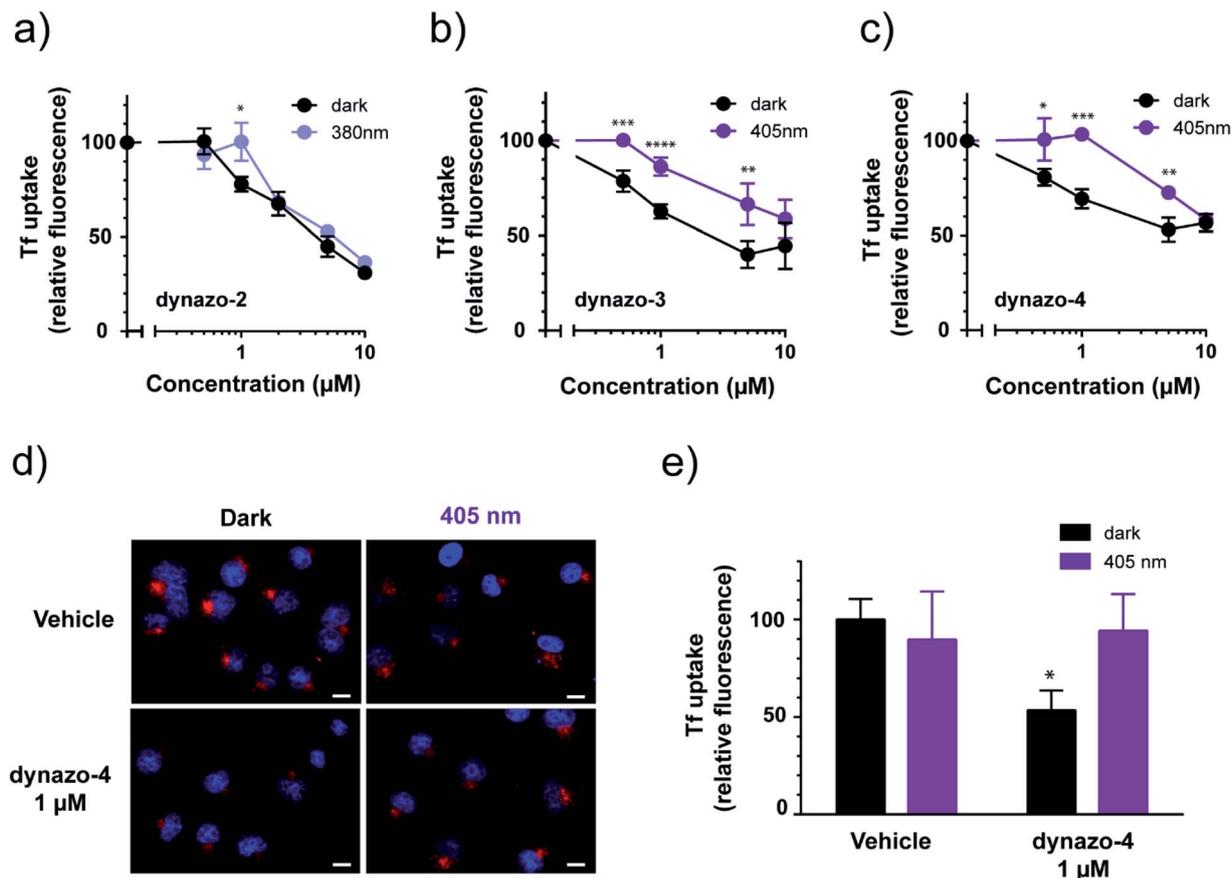
Fig. 3 Characterization of dynazos' biological activity. (a) Dose−response curve of Tf uptake by flow cytometry in the dark and under illumination at 380 nm for dynazo-**2** shows dose-dependent inhibition of Alexa-488-Tf uptake and significant differences in activity with light at 1 μM (*$P < 0.05$). (b) Dynazo-**3** and (c) dynazo-**4** dose−response curves in the dark and under illumination at 405 nm show dose-dependent inhibition and significant differences in activity with light between 0.5–5 μM (*$P < 0.05$, **$P < 0.01$, ***$P < 0.001$, ****$P < 0.0001$). In all these cases, dose−response curves were normalized to those measured for vehicle-treated samples (100%). Data are representative of three independent experiments performed in duplicate and values are expressed in mean ± SEM. (d) Confocal microscopy images of Tf uptake assays in the dark and at 405 nm irradiation shows a significant reduction in Alexa-568-Tf uptake only in cells treated with dynazo-**4** (1 μM) in the dark condition. Internalized Tf is shown in red and DRAQ5 blue staining shows nuclei (scale bar: 10 μm). Quantification of Tf uptake assay from (d) [normalized to vehicle-treated in the dark (100%)] is shown in (e) (*$P < 0.05$, $n = 112$ cells for vehicle/dark, $n = 122$ cells for vehicle/405 nm, $n = 151$ for dynazo-**4** 1 μM/dark and $n = 153$ cells for dynazo-**4** 1 μM/405 nm). All data are expressed as the mean ± SEM.

inhibitors of dynamin) that are directly applied to the bath. Dynazos are active at 1 μM concentration in the dark and can be deactivated to different extents with violet illumination, which may produce significantly lower toxicity and less unspecific effects than dynasore at the usual 80 μM concentration. In particular, at 1 μM concentration dynazo-**4** can inhibit CME up to 47% and be photoswitched to a fully inactive state using an illumination wavelength available in most commercial laser scanning microscopes.

We also assessed the capacity of dynazo-**4** to photocontrol the dynamics of clathrin-coated pit (CCP) formation during endocytosis. To this end, we used live-cell total internal reflection fluorescence microscopy (TIRFM) to monitor the CCP lifetimes by tracking the fluorescently labeled AP-2 protein in BSC-1 cells, using customized particle-tracking software.[37] Together with clathrin, AP-2 is the most abundant coat protein in the CCP and it is also present during the entire lifetime of a CPP.[38,39] We recorded time lapse movies of BSC-1 cells

expressing the eGFP-tagged adaptor protein AP-2 before and after the incubation with 25 μM dynazo-**4** for 40 minutes. Following, we recorded the CCP dynamics under continuous 405 nm illumination in the presence of dynazo-**4** (ESI Fig. S6–S8†). Dynazo-**4** treatment significantly increases the time duration of the CCP at the plasma membrane, indicating a slowdown of the endocytic process in full agreement with transferrin uptake assays by flow cytometry and fluorescence microscopy (Fig. 3). This effect is reversible under 405 nm illumination in the case of the CCP with a time duration of ≥120 seconds, but not at shorter time durations, probably due to the fast relaxation lifetime of dynazo-**4**, which limits the effective percentage of (inactive) *cis* isomer that can be achieved under illumination (ESI Fig. S7c†). These differences could also be due to the absence of dynamin recruitment in some CCP pools, which accelerates their disappearance from the plasma membrane.[40] Control experiments in untreated cells showed no effect of 405 nm illumination on CCP lifetime (ESI Fig. S7d†).

Compared to traffic light peptides,[37] dynazo-**4** targets a protein bearing wider impact in endocytosis, it achieves comparable photocontrol of CME at 20-fold lower concentration, it has 4.6-fold smaller molecular weight (609.63 Da compared to 2830.8 Da of TL-2) and simpler synthetic accessibility.

Due to the rapid *cis* to *trans* relaxation of dynazos, we could not estimate the content of the *cis* isomer in the illuminated sample. According to the results in Fig. 2, it is likely that the *cis*/*trans* mixture in the PSS of illuminated dynazos contains a residual fraction of the more active isomer (*trans*) that is sufficiently high to limit the range of concentrations displaying light-dependent inhibition of Tf uptake. Reducing the *trans* isomer content in the PSS of illuminated dynazos (*i.e.* photo-converting more efficiently to the *cis* state) would likely enhance the differences in activity between the *cis*/*trans* forms, thereby expanding the useful concentration range of dynazos.

In addition, an enhancement of the photoswitchable steric hindrance around the pharmacophore with even bulkier substituents could further reduce the activity of *cis* isomers and increase *cis*/*trans* differential biological activity. It is worth noting that the inhibition of endocytosis by 1 μM dynazo-**4** can be completely shut off under illumination, despite partial photoconversion (Fig. 3c). However, it would also be useful for certain experiments that the inactive isomer was most abundant in the dark, and that endocytosis could be inhibited with light (*e.g.* at focalized spots). This could in principle be achieved by means of a "reverse switch" with a bridged azobenzene which adopts a more stable *cis* configuration in the dark,[41] although in turn, the resulting compound may display partial (basal) inhibition in the relaxed form instead of the complete inactivity of *cis*-dynazo-**4**. On the other hand, the large separation of the *cis* and *trans* absorbance bands in bridged azobenzenes should enable complete bidirectional switching with violet/green light.

Conclusions

In summary, we have used rational design to obtain the first light-regulated small-molecule inhibitor of endocytosis. Integration of substituted azobenzenes in the structure of dynasore while preserving the integrity of its pharmacophore is a successful strategy to endow photosensitivity to a dynamin inhibitor. In a series of stepwise modifications of the azo-benzene core, first we have red-shifted the photoisomerization wavelength of dynazos in order to uncouple it from dynasore absorption, prevent photodegradation, and allow the use of visible light to switch off their activity. And second, we have blocked the activity of the *cis* isomer and enhanced functional photoswitching by increasing the steric hindrance around the pharmacophore and reducing the affinity of the *cis* isomer for its target. All compounds in the series are active in living cells and can be photomodulated to different extents. Remarkably, the activity of dynazos in living cells indicates that these dynasore derivatives are also cell-permeable compounds. These results constitute the proof of principle for the development of optimized photoswitchable dynasore analogs to manipulate dynamin-dependent endocytosis. These photopharmacological tools can be useful to dissect the role of endocytosis in cellular functions where it exerts a crucial role, such as cell growth, differentiation, cell motility and invasiveness, modulation of transmembrane receptor signalling and synaptic transmission.

Conflicts of interest

There are no conflicts to declare.

Acknowledgements

Notes and references

1 S. L. Schreiber, J. D. Kotz, M. Li, J. Aubé, C. P. Austin, J. C. Reed, H. Rosen, E. L. White, L. A. Sklar, C. W. Lindsley, B. R. Alexander, J. A. Bittker, P. A. Clemons, A. De Souza, M. A. Foley, M. Palmer, A. F. Shamji, M. J. Wawer, O. McManus, M. Wu, B. Zou, H. Yu, J. E. Golden, F. J. Schoenen, A. Simeonov, A. Jadhav, M. R. Jackson, A. B. Pinkerton, T. D. Y. Chung, P. R. Griffin, B. F. Cravatt, P. S. Hodder, W. R. Roush, E. Roberts, D. H. Chung, C. B. Jonsson, J. W. Noah, W. E. Severson, S. Ananthan, B. Edwards, T. I. Oprea, P. J. Conn, C. R. Hopkins, M. R. Wood, S. R. Stauffer and K. A. Emmitte, *Cell*, 2015, **161**, 1252–1265.

2 T. G. Iversen, G. Skretting, B. Van Deurs and K. Sandvig, *Proc. Natl. Acad. Sci. U. S. A.*, 2003, **100**, 5175–5180.

3 M. Izquierdo-Serra, A. Bautista-Barrufet, A. Trapero, A. Garrido-Charles, A. Diaz-Tahoces, N. Camarero, S. Pittolo, S. Valbuena, A. Perez-Jimenez, M. Gay, A. Garcia-Moll, C. Rodriguez-Escrich, J. Lerma, P. De La Villa, E. Fernandez, M. A. Pericas, A. Llebaria and P. Gorostiza, *Nat. Commun.*, 2016, **7**, 12221.

4 Y. Posor, M. Eichhorn-Gruenig, D. Puchkov, J. Schöneberg, A. Ullrich, A. Lampe, R. Müller, S. Zarbakhsh, F. Gulluni, E. Hirsch, M. Krauss, C. Schultz, J. Schmoranzer, F. Noé and V. Haucke, *Nature*, 2013, **499**, 233–237.

5 W. A. Velema, W. Szymanski and B. L. Feringa, *J. Am. Chem. Soc.*, 2014, **136**, 2178–2191.

6 N. Carelle, E. Piotto, A. Bellanger, J. Germanaud, A. Thuillier and D. Khayat, *Cancer*, 2002, **95**, 155–163.

7 J. Broichhagen, J. A. Frank and D. Trauner, *Acc. Chem. Res.*, 2015, **48**(7), 1947–1960.

8 X. Gómez-Santacana, S. Pittolo, X. Rovira, M. Lopez, C. Zussy, J. A. R. Dalton, A. Faucherre, C. Jopling, J. P. Pin, F. Ciruela, C. Goudet, J. Giraldo, P. Gorostiza and A. Llebaria, *ACS Cent. Sci.*, 2017, **3**, 81–91.

9 P. Gorostiza, M. Volgraf, R. Numano, S. Szobota, D. Trauner and E. Y. Isacoff, *Proc. Natl. Acad. Sci. U. S. A.*, 2007, **104**, 10865–10870.

10 R. H. Kramer, A. Mourot and H. Adesnik, *Nat. Neurosci.*, 2013, **16**, 816–823.

11 J. Broichhagen, M. Schönberger, S. C. Cork, J. A. Frank, P. Marchetti, M. Bugliani, A. M. J. Shapiro, S. Trapp, G. A. Rutter, D. J. Hodson and D. Trauner, *Nat. Commun.*, 2014, **5**, 5116.

12 S. Pittolo, X. Gómez-Santacana, K. Eckelt, X. Rovira, J. Dalton, C. Goudet, J. P. Pin, A. Llobet, J. Giraldo, A. Llebaria and P. Gorostiza, *Nat. Chem. Biol.*, 2014, **10**, 813–815.

13 M. Schönberger and D. Trauner, *Angew. Chem., Int. Ed.*, 2014, **53**(12), 3264–3267.

14 B. Schierling, A. J. Noel, W. Wende, T. Hien le, E. Volkov, E. Kubareva, T. Oretskaya, M. Kokkinidis, A. Rompp, B. Spengler and A. Pingoud, *Proc. Natl. Acad. Sci. U. S. A.*, 2010, **107**, 1361–1366.

15 W. Szymanski, M. E. Ourailidou, W. A. Velema, F. J. Dekker and B. L. Feringa, *Chem.–Eur. J.*, 2015, **21**, 16517–16524.

16 A. A. Beharry and G. A. Woolley, *Chem. Soc. Rev.*, 2011, **40**, 4422–4437.

17 C. B. Harper, M. R. Popoff, A. McCluskey, P. J. Robinson and F. A. Meunier, *Trends Cell Biol.*, 2013, **23**, 90–101.

18 G. J. Doherty and H. T. McMahon, *Annu. Rev. Biochem.*, 2009, **78**, 857–902.

19 M. Mettlen, P.-H. Chen, S. Srinivasan, G. Danuser and S. L. Schmid, *Annu. Rev. Biochem.*, 2018, **87**, 871–896.

20 A. I. Ivanov, *Methods Mol. Biol.*, DOI: 2014, 1174, 3-18.

21 G. J. Doherty and H. T. McMahon, *Annu. Rev. Biochem.*, 2019, **78**, 857–902.

22 S. M. Ferguson and P. De Camilli, *Nat. Rev. Mol. Cell Biol.*, 2012, **13**, 75–88.

23 S. Mayor, R. G. Parton and J. G. Donaldson, *Cold Spring Harbor Perspect. Biol.*, 2014, **6**, a016758.

24 H. T. McMahon and E. Boucrot, *Nat. Rev. Mol. Cell Biol.*, 2011, **12**, 517–533.

25 A. Mccluskey, J. A. Daniel, G. Hadzic, N. Chau, E. L. Clayton, A. Mariana, A. Whiting, N. N. Gorgani, J. Lloyd, A. Quan, L. Moshkanbaryans, S. Krishnan, S. Perera, M. Chircop, L. von Kleist, A. B. Mcgeachie, M. T. Howes, R. G. Parton, M. Campbell, J. A. Sakoff, X. Wang, J. Y. Sun, M. J. Robertson, F. M. Deane, T. H. Nguyen, F. A. Meunier, M. A. Cousin and P. J. Robinson, *Traffic*, 2013, **14**, 1272–1289.

26 M. J. Robertson, G. Hadzic, J. Ambrus, D. Y. Pomè, E. Hyde, A. Whiting, A. Mariana, L. Von Kleist, N. Chau, V. Haucke, P. J. Robinson and A. McCluskey, *ACS Med. Chem. Lett.*, 2012, **3**(5), 352–356.

27 A. Quan, A. B. McGeachie, D. J. Keating, E. M. Van Dam, J. Rusak, N. Chau, C. S. Malladi, C. Chen, A. McCluskey, M. A. Cousin and P. J. Robinson, *Mol. Pharmacol.*, 2007, **72**, 1425–1439.

28 E. Macia, M. Ehrlich, R. Massol, E. Boucrot, C. Brunner and T. Kirchhausen, *Dev. Cell*, 2006, **10**, 839–850.

29 T. Hill, L. R. Odell, J. K. Edwards, M. E. Graham, A. B. McGeachie, J. Rusak, A. Quan, R. Abagyan, J. L. Scott, P. J. Robinson and A. McCluskey, *J. Med. Chem.*, 2005, **48**, 7781–7788.

30 S. Lee, K. Y. Jung, J. Park, J. H. Cho, Y. C. Kim and S. Chang, *Bioorg. Med. Chem. Lett.*, 2010, **20**, 4858–4864.

31 J. Forman, M. Dietrich and W. Todd Monroe, *Photochem. Photobiol. Sci.*, 2007, **6**, 649–658.

32 Q. Dong, K. Svoboda, T. R. Tiersch and W. Todd Monroe, *J. Photochem. Photobiol., B*, 2007, **88**, 137–146.

33 H. M. D. Bandara and S. C. Burdette, *Chem. Soc. Rev.*, 2012, **41**, 1809–1825.

34 N. J. Dunn, W. H. Humphries IV, A. R. Offenbacher, T. L. King and J. A. Gray, *J. Phys. Chem. A*, 2009, **113**(47), 13144–13151.

35 T. Kirchhausen, E. Macia and H. E. Pelish, *Methods Enzymol.*, 2008, **438**, 77–93.

36 M. Izquierdo-Serra, M. Gascón-Moya, J. J. Hirtz, S. Pittolo, K. E. Poskanzer, È. Ferrer, R. Alibés, F. Busqué, R. Yuste, J. Hernando and P. Gorostiza, *J. Am. Chem. Soc.*, 2014, **136**(24), 8693–8701.

37 L. Nevola, A. Martín-Quirõs, K. Eckelt, N. Camarero, S. Tosi, A. Llobet, E. Giralt and P. Gorostiza, *Angew. Chem., Int. Ed.*, 2013, **52**, 7704–7708.

38 M. Mettlen, P.-H. Chen, S. Srinivasan, G. Danuser and S. L. Schmid, *Annu. Rev. Biochem.*, 2018, **87**, 871–896.

39 M. Mettlen and G. Danuser, *Cold Spring Harbor Perspect. Biol.*, 2014, **6**, a017038.

40 F. Aguet, C. N. Antonescu, M. Mettlen, S. L. Schmid and G. Danuser, *Dev. Cell*, 2013, **26**(3), 279–291.

41 S. Samanta, C. Qin, A. J. Lough and G. A. Woolley, *Angew. Chem., Int. Ed.*, 2012, **51**, 6452–6455.